Arab J Geosci
DOI 10.1007/s12517-013-1021-3

ORIGINAL PAPER

Estimation of source parameters and attenuation using digital waveforms of Al-Ays 2009 earthquake, Saudi Arabia

A. K. Abdel-Fattah · A. M. Al-Amri · M. S. Fnais · kamal Abdelrahman

Received: 1 April 2013 / Accepted: 24 June 2013

Abstract On 19 May 2009, an earthquake sequence of M_w=4.8 occurred at 25.20°N 37.76°E about 60 km onshore of the Red Sea coastline, Saudi Arabia. In the present study, the digital waveform data from the largest four events were used to estimate the source parameters and attenuation characteristics along the source-to-station path in the Arabian Shield. A grid search technique, combined with an assumption of circular source model, was applied to find the best-fit spectral amplitude over the space parameters: long period spectral level (Ω_0), corner frequency (f_0) and asymptotic high-frequency fall-off (γ). Consequently, the spectral parameters were used to estimate source parameters: seismic moment, fault radius (assumed circular rupture model) and stress drop. Seismic moments are founded to be within the range of 2.34E+14 to 2.83E+16 Nm and their corresponding moment magnitudes range from 3.5 to 4.8; the fault radius ranges from 369 to 1,498 m, and stress drops are observed in the range of 8.7 to 32.0 b. The spectral slopes beyond the corner frequency displayed $\omega^{-2.4}$ to $\omega^{-2.6}$ behaviours in contrast with Brune's source model of ω^{-2}. This finding requires more detailed investigations on large data sets to distinguish the behaviour mechanism of the spectral slopes at high frequencies. By taking the ratio between observed and calculated spectra, the attenuation curves for P and S waves were derived along the source-to-station paths. The preliminarily results exhibited high quality factors of Q_α=3,883 and Q_β=3,530 for P and S waves, respectively. To this end, the ratio Q_β/Q_α is founded to be slightly less than unity indicating that the body waves from source-to-station paths crossed a crustal volume that is partially saturated with fluids causing lower attenuation effect on *P* waves than on S waves in the Arabian Shield.

Keywords Arabian Shield · Earthquake source parameters · Body wave attenuation · Saudi Arabia

A. K. Abdel-Fattah · A. M. Al-Amri · M. S. Fnais · k. Abdelrahman
Geology and Geophysics Department, Faculty of Science, King Saud University, Riyadh, Saudi Arabia

A. K. Abdel-Fattah (✉) · k. Abdelrahman
National Research Institute of Astronomy and Geophysics (NRIAG), 11421 Helwan, Cairo, Egypt
e-mail: aabdelfattah@ksu.edu.sa

Present Address:
A. K. Abdel-Fattah
Geology and Geophysics Department, College of Science, King Saud University, Riyadh, Saudi Arabia

Introduction

The Arabian Peninsula is surrounded by relatively high active tectonic zones: the Gulf of Aden and Red Sea spreading zones, Dead Sea Transform fault zone, East Anatolian fault, Bitlis and Zagros suture zones, Makran thrust fault and Owen fracture zone, as shown in Fig. 1. The plate boundaries are capable to generate large seismic events of magnitude 7+ (e.g. the 1967 M7.0 earthquake in the Gulf of Aden, the 1971 M7.0 earthquake in the Bitlis zone, the 1972 M7.0 earthquake in the Zagros suture zone and the 1995 M7.2 earthquake in the Gulf of Aqaba). The seismic activity is not only distributed along the plate boundary but also is extended to take place inside the Arabian Plate, as shown in Fig. 2. Over the historic record, the Arabian Shield has experienced three earthquakes associated with volcanic eruptions (641, 1256 and possibly in 1800 AD). Along the onshore, the region has recently suffered from three earthquakes which occurred in Tabuk area (2004), Badr area (2009) and Al-Ays volcanic zone (2007 and 2009). The earthquakes were felt by local resistance in the vicinity of the epicentral areas. The focal mechanism solutions of Tabuk, Bader and Al-Ays earthquakes show normal faulting mechanism with two nodal planes oriented NW-SE, parallel to the Red Sea, as determined by Al-

Published online: 21 August 2013

Damegh et al. (2009, 2010) and Craig et al. (2011), respectively. The strike of the fault planes agrees well with the surface observations of NW trending faults, interpreted to be a part of the Najd Fault System (Al-Damegh et al. 2010). The stress field of the Tabuk, Badr and Al-Ays events is characterised by a nearly horizontal NE-SW extension. The epicentres and the focal mechanism solutions of the recent three earthquakes are shown in Fig. 3. These earthquakes emphasised the importance of defining the input parameters needed for the reassessment of seismic hazards in the western part of Saudi Arabia on the basis of the recent geophysical, geological and seismological database.

The present study focuses on analysing the digital waveform of the largest four earthquakes that occurred in Al-Ays seismic zone in May 2009. Al-Ays dislocation zone is associated with the Harrat Lunayyir volcanic field, northern Arabian Shield, Saudi Arabia (Fig. 2). Although the seismicity occurring in the zone is identified by many authors as intraplate earthquake swarm activity, the origin of the peculiar seismicity is not well known, whether it is triggered by magma intrusion into the extensional faulting, tectonic process or a temporal coupling process of mechanical interaction between tectonic and magnetic potential. However, intraplate earthquake swarms are usually observed in the areas of active volcanisms. Moreover, they occur mainly in the areas of enhanced crustal fluid activity, particularly in regions with the Quaternary volcanism. The occurrence of swarms is explained by the intrusion of crustal fluids into the fault zone or by a seismic slip (Vidale and Shearer 2006). Fluid activity can be due to periodic dyke intrusions that generate stress heterogeneity near the fracture zone. Recently, precise hypocentral distributions around volcanoes and active faults showed a linear alignment caused by a fault tip (Got et al. 1994; Rubin et al. 1999; Waldhauser et al. 1999), by structural weakness (Gillard et al. 1996) and by an intruded dyke (Rubin et al. 1998). The occurrence of intraplate earthquake swarms is usually explained by coupling activity of tectonic stress and the existence of highly pressurised pore fluids in subcritically loaded rocks. The dyke intrusion model supported the coupling mechanism of the seismotectonics and pore pressure diffusion processes.

On 19 May 2009 at 17:34 (UTC), a moderate-sized earthquake occurred in Al-Ays zone with moment magnitude of 4.8 (Craig et al. 2011) comprising approximately 4,000 events of shallow depths in the range of 5–20 km and micro-to-small-sized magnitudes, as reported by Saudi Geological Survey (SGS) website. As a matter of fact, earthquake swarms are characterised by the magnitude of the largest

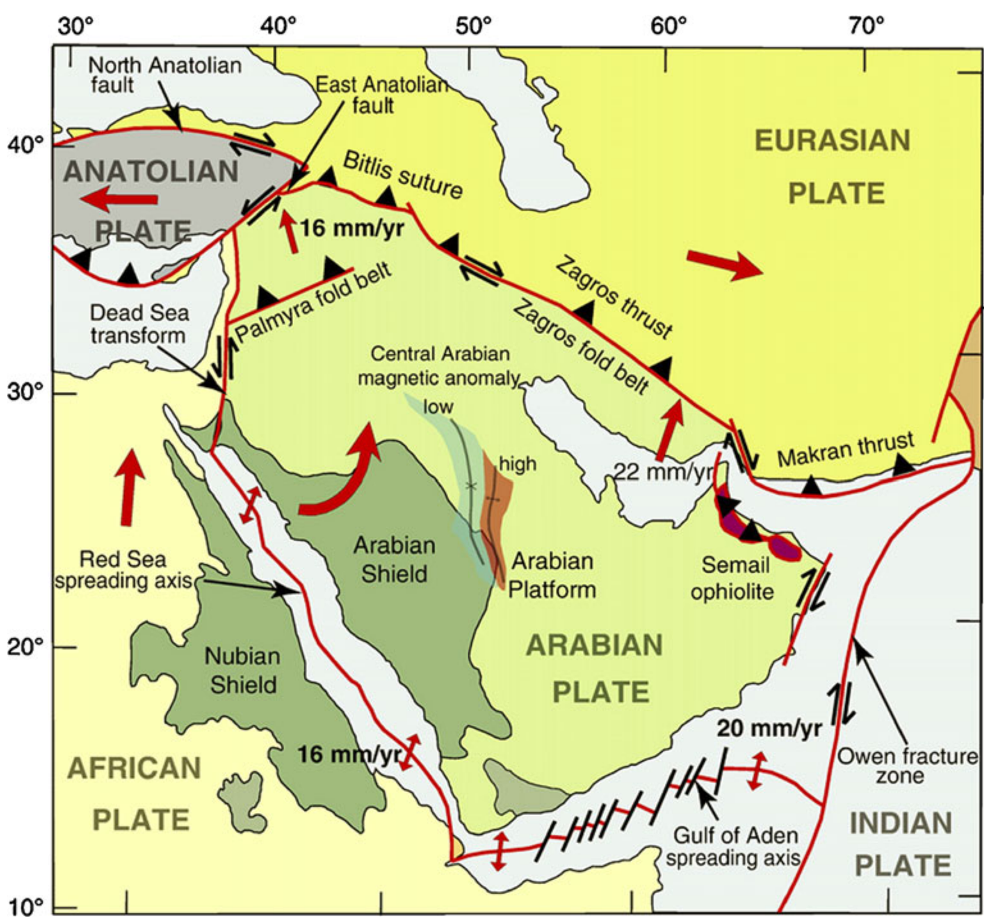

Fig. 1 Simplified map of the Arabian Plate, with plate boundaries, approximate plate convergence vectors and principal geologic features (after Stern and Johnson 2010)

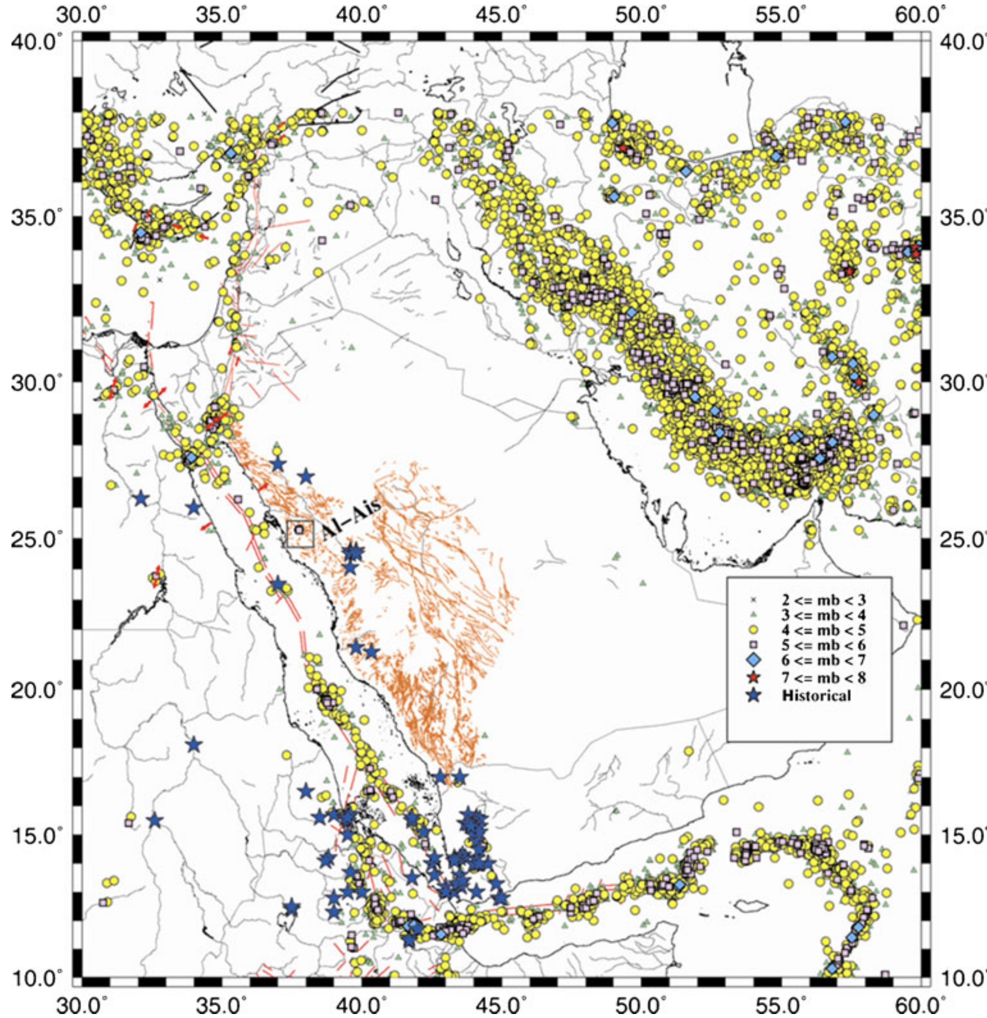

Fig. 2 Seismicity of the Arabian plate and its surroundings as compiled for instrumental seismicity from ISC (1964–2012) while historical earthquake data (827–1906) were compiled from many authors (e.g. Adams and Barazangi 1984; Camp et al. 1991; Bosworth et al. 2005; Poirier and Taher 1980; Ambraseys et al. 1994). The *open square* denotes the Al-Ays dislocation zone

events which rarely observed to exceed the M5.0 for intraplate earthquake swarms. Previous studies of the epicentral area after the occurrence of the respective earthquake using satellite interferometry indicated that the sequence was associated with dyke injection parallel to the margin (Baer and Hamiel 2010; Pallister et al. 2010). The epicentres are aligned NNW as shown in Fig. 4. The hypocentres can be grouped into two sets according to focal depths (Fig. 4); deeper events located in the southern part of the region while the shallower events at the north. The hypocentral distributions accompanied by surface deformations supported the dyke intrusion model beneath the epicentral area. An incipient status of dyke intrusion is suggested by modelling results for the 2009 Al-Ays earthquake swarm (Mukhopadhyay et al. 2012).

The present study aims to estimate source parameters of 19 May 2009 earthquake and to preliminarily calibrate the attenuation along the whole path for the seismic stations located on the stable Arabian Shield. The determination of earthquake source parameters is of particular interest in complex geodynamic environments, such as Harrat Lunayyir, where the seismicity is characterised by small-sized earthquakes not accompanied with large earthquakes. The evaluation of seismic attenuation represents a key role for the quantitative estimation of the parameters which control the propagation of elastic waves and the source processes acting inside complex tectonic areas. The results are of great importance to use for the potential hazard assessment of Al-Ays earthquake prone area.

Tectonic settings

The seafloor spreading along the Red Sea is attributed to continental extension and rifting which resulted from the northward motion of the Arabian Plate relative to the African Plate (Fig. 1). On the eastern margin of the Red Sea, where the Arabian Shield is spatially extended, the region is characterised by dynamic elevation of topography which is believed to be associated with upwelling in the underlying mantle (e.g. Daradich et al. 2003). Increased seismic activity

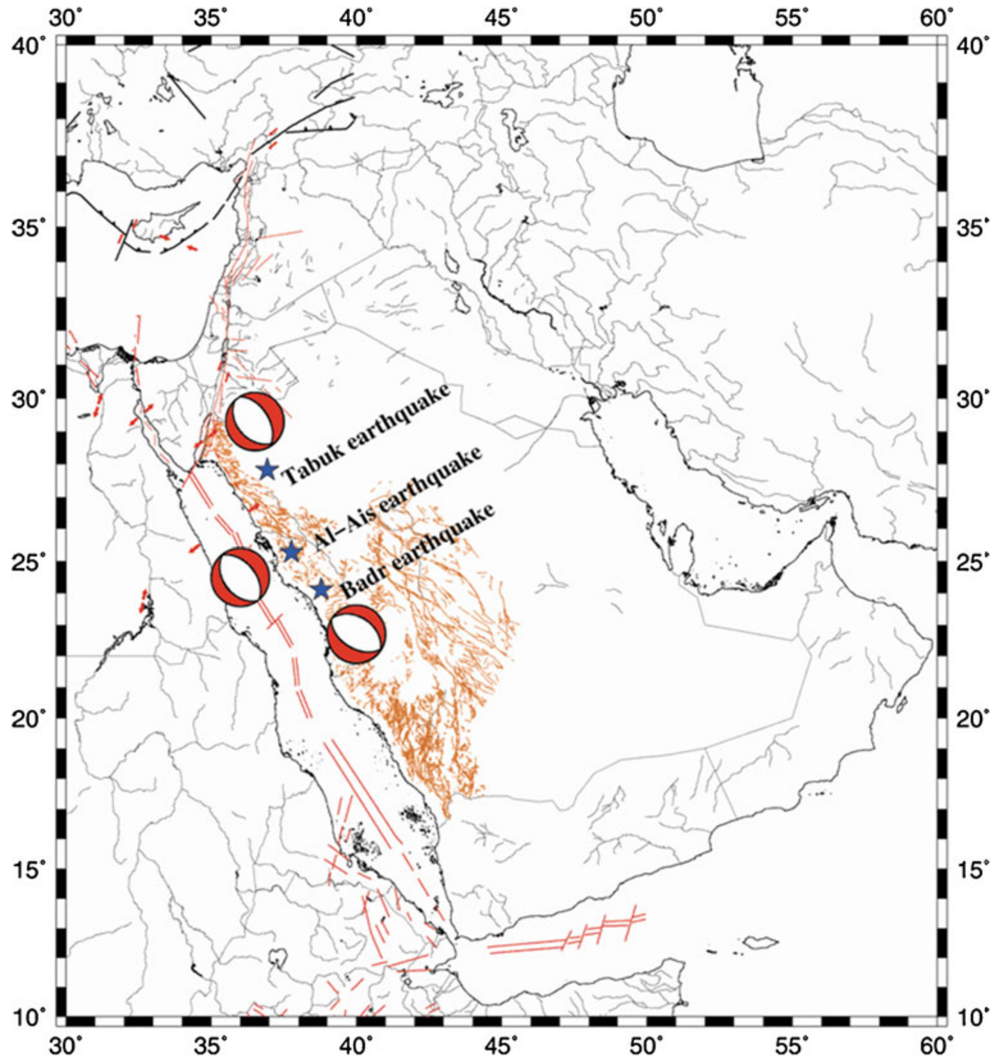

Fig. 3 Focal mechanism solutions of recent three earthquakes, Tabuk 2004, Badr 2009 and Al-Ays 2009, which occurred on the Arabian Shield, onshore of the eastern Red Sea coastline

along the Arabian margin of the Red Sea, in contrast to the African side, corresponds to a marked difference in the elevated topography reflecting a large free-air gravity anomaly along the Arabian margin which is not present under the African margin (Craig et al. 2011). The uplifting and volcanism in the Arabian Shield are generally assumed to be the result of hot, buoyant material in the upper mantle that may have eroded the base of the lithosphere (Camp and Roobol 1992). Previous studies suggested that the reduction of seismic wave velocities are related to the presence of thermal mantle lithosphere beneath the shield (Debayle et al. 2001; Benoti et al. 2003; Nyblade et al. 2006; Park et al. 2007, 2008; Al-Amri et al. 2008; Chang and Van der Lee 2011). The mantle plume was recognised beneath the western part of the Arabian plate including Harrat Lunayyir (Benoti et al. 2003; Daradich et al. 2003; Julia et al. 2003; Al-Damegh et al. 2005) with surface evidence of ocean–island basalt volcanism (Moufti and Hashad 2005). The positive gravity anomalies associated with low seismic velocities and dynamic elevated topography reflected that the region has been subjected to magmatic lithosphere causing the increasing of topographic elevation.

The epicentral area belongs to one of the western Arabia lava fields (Harrat Lunayyir) in the Arabian Shield. The area is almost characterised by Cenozoic flood basaltic flows reaching the ground surface through the prevailing deep cracks and fissures since Miocene. The region is dominated by NW-striking dykes and faults of NS to NE-SW and EW-striking fault systems (Brown 1972). The region is tectonically undergoing extension as a result of normal faulting mechanisms of dipping planes towards and away from the Red Sea coastal plain (Roobol 2007). The focal mechanism determined by Craig et al. (2011) and Harvard Global Centroid Moment Tensor Catalogue (http://www.globalcmt.org/CMTsearch.html) showed normal faulting mechanism of two nodal planes oriented NW-SE. This type of mechanism is common with the earthquakes occurring in the north western Saudi Arabia and is in consistence with the faults

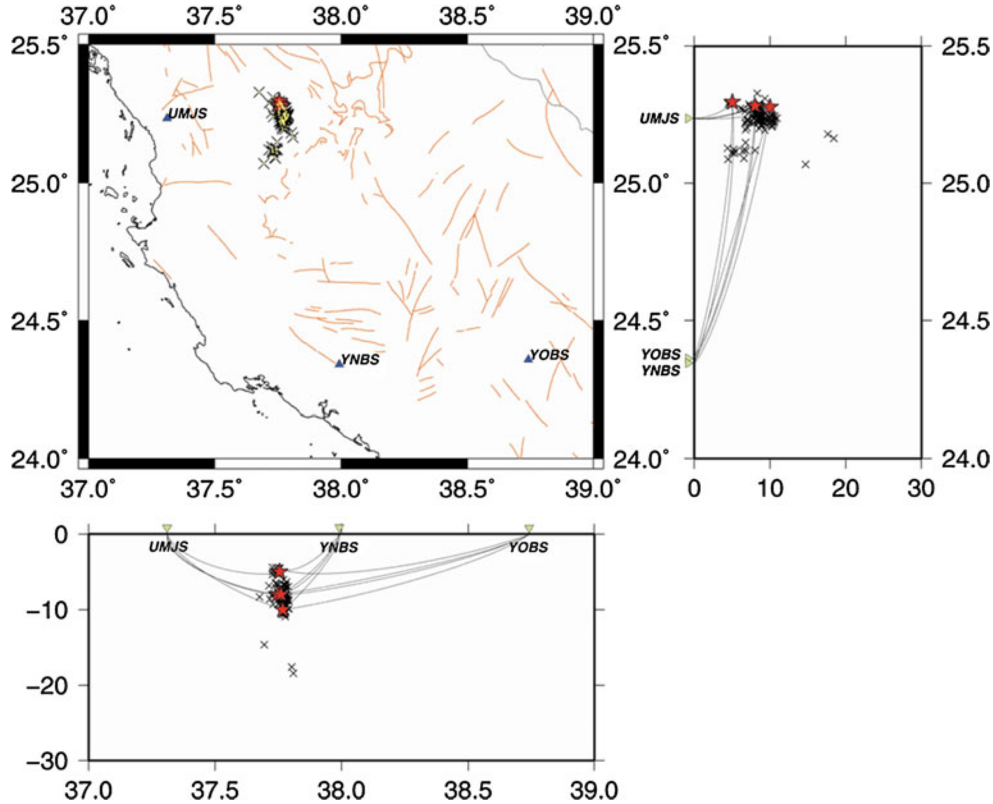

Fig. 4 Locations of hundred earthquakes (*crosses*) as determine by SGS, *solid stars* displayed locations of four earthquakes, as determine by USGS, used in the present study. The figure shows also the permanent seismic stations (*solid triangles*) which their digital waveform data used to estimate source parameters and to calibrate the attenuation characteristics along the source-to-station paths (*bright black lines*)

near the epicentre area. The mechanism reflects the dominantly northeast extensional tectonic regime in the province.

Data analysis

On 19 May 2009, a moderate-sized earthquake of moment magnitude 4.8 occurred approximately 60 km east of the Red Sea coastline, Al-Ays volcanic zone, Harrat Lunayyir, western Saudi Arabia. The mainshock of M_w 4.8 (Craig et al. 2011) was strongly felt by local residents of Al-Ays town and its vicinity. The epicentre was located at 25.282°N latitude, 37.7597°E longitude and shallow source depth of 4 km. The mainshock is considered as the largest recorded earthquake in the region. Surface deformations with different directions and extensions were associated with the event.

The earthquake hypocentral locations, fault plane solutions and the seismic stations are shown in Fig. 4. The respective events were only observed at three seismic stations: UMLJ, YNBS and YOBS. The focal mechanisms and hypocentral parameters are listed in Table 1. The hypocentral parameters were determined by SGS using the HYPOINV2000 and a number of observations included both P and S arrival times. For the mainshock, the focal mechanism and the focal depth were estimated by using waveform inversion technique (Craig et al. 2011). For the other three events, the focal depths and fault plane solutions were resolved by USGS. The waveform data of the mainshock are shown in Fig. 5.

Spectral amplitudes are routinely estimated in the frequency domain using a transform technique such as fast Fourier transform (FFT). Waveform data recorded by a few numbers of broadband seismic stations operating by SGS few hours before the occurrence of the mainshock were used to estimate spectral amplitudes of Al-Ays earthquake and to investigate the attenuation characteristics of body seismic waves. The stations UMJS and YOBS are equipped with a Trillium 40s velocity sensor having an approximately flat response from 0.02 to 40 s. While station YNBS is equipped with a Trillium 120s velocity sensor having a response range of 0.02–120 s. The signal sampling frequency is 100 Hz for all and the dynamic range of the whole recording system is approximately 142 dB.

In the present study, the records were corrected to zero baseline and instrument response. Time windows for both P and S waves were manually selected using the generic mouse of PGPLOT subroutines through X Window graphical user interface to avoid contamination from other phases and maintain the resolution and stability of the spectra. Shadow areas in Fig. 5 refer to the selected windows for P and S waves used in spectral parameter estimations. Second-order high-pass Butterworth filter of 0.5 Hz corner frequency was applied before the FFT to remove the long period biases from the waveform data set. The east–west and north–south

Table 1 The focal mechanism and hypocentral parameters of the study events

ID	Date			Origin Time			Location		H [km]	M_w	Fault plane		
	Year	Month	Day	Hour	Minute	Second	Latitude [°]	Longitude [°]			φ [°]	δ [°]	λ [°]
1	2009	05	19	06	38	33.30	25.2818	37.7478	08	3.5	337	43	−73
2	2009	05	19	16	54	31.70	25.2763	37.7677	10	3.8	329	48	−87
3	2009	05	19	17	35	02.50	25.2820	37.7597	08	4.8	144	45	−93
4	2009	05	19	19	57	19.50	25.2955	37.7552	05	4.0	330	46	−64

H depth, M_w moment magnitude, φ strike, δ dip, λ rake

components are combined in the Fourier domain to obtain a single horizontal component:

$$S(f) = \sqrt{S_{NS}\frac{(f)^2 + S_{EW}(f)^2}{2}} \tag{1}$$

A cosine taper was applied to the time series while the weighting function (Konno and Ohmachi 1998) was applied to smooth the amplitude spectrum over long-spaced abscissa values of smooth parameter of 0.2.

Source parameters and whole path attenuation factor estimations

The seismic source spectra are estimated from the analysis of the P and S waves recorded at seismic stations using an approximation of source model and one of regression techniques. Using a point–source approximation, the spectral amplitude for an event can be written as

$$A_i(f) = C{\cdot}S_i(f){\cdot}G(R){\cdot}e^{-\pi f t / Q} \tag{2}$$

where C is a scaling factor, $S_i(f)$ is the source spectrum, $G(R)$ is the geometrical spreading term, R is the hypocentral distance and Q is the quality factor. The source velocity spectrum, $S_i(f)$ can be modelled following an analytical approximation such as introduced by Brune (1970) and Boatwright (1978). The general model is given by;

$$S_i(f) = \frac{2\pi f \cdot \Omega_0}{\sqrt{1 + \left({}^{f}/_{f_0}\right)^{2\gamma}}} \tag{3}$$

where Ω_0 is the low-frequency spectral level, f_0 is the corner frequency (e.g. Brune 1970) and γ is the asymptotic high-frequency spectral decay that is bounded between 1 (required for conservation of seismic energy) and 3 based on how fast the signal decays above the corner frequency controlled by the cubic model that assumed the similarity in high-frequency energy releasing from small and large earthquakes.

Estimates of these spectral parameters can subsequently be used to estimate parameters not directly measurable in the data such as, seismic moment, fault radius (assumed circular rupture) and stress drop. Stress drop is a key parameter needed to understand the physics of earthquakes, investigate seismic source scaling behaviours and infer local stress characteristics in the crust (Imanishi et al. 2004).

The best-fit model was determined by minimising the miss-fit function, based on L_1 norm, between the observed amplitude spectrum and the calculated one,

$$\|\log(S_i(f)) - \log(A_i(f))\|_{L_1} = \min \tag{4}$$

An iterative technique was applied to find the best-fit by a grid search over Ω_0, f_0 and γ. The search was grossly iterated starting around an average values over γ incrementing by 0.5, f_0 incrementing by 2 and Ω_0 incrementing by 1. A fine search was focused in a narrow range around the minimum misfit values. The first approximation of f_0 and Ω_0 were calculated using the method of Snoke (1987):

$$J = 2\int_0^\infty |V(w)|^2 df \tag{5}$$

$$K = 2\int_0^\infty |\,U(w)|^2 df \tag{6}$$

$$\Omega_0^1 = 2\left(\frac{K^3}{J}\right)^{1/4} \tag{7}$$

$$f_0^1 = \frac{1}{2\pi}\sqrt{\left(\frac{J}{K}\right)} \tag{8}$$

where $U(w)$ and $V(w)$ are the displacement spectrum and ground velocity spectrum, respectively. Figure 6 displays examples of P and S wave spectra and their fitted source model from the mainshock data set recorded by the UMJS, YNBS and YOBS seismic stations. The space model parameters converged the best fits of the spectral amplitudes that were converted to estimate the source parameters by their

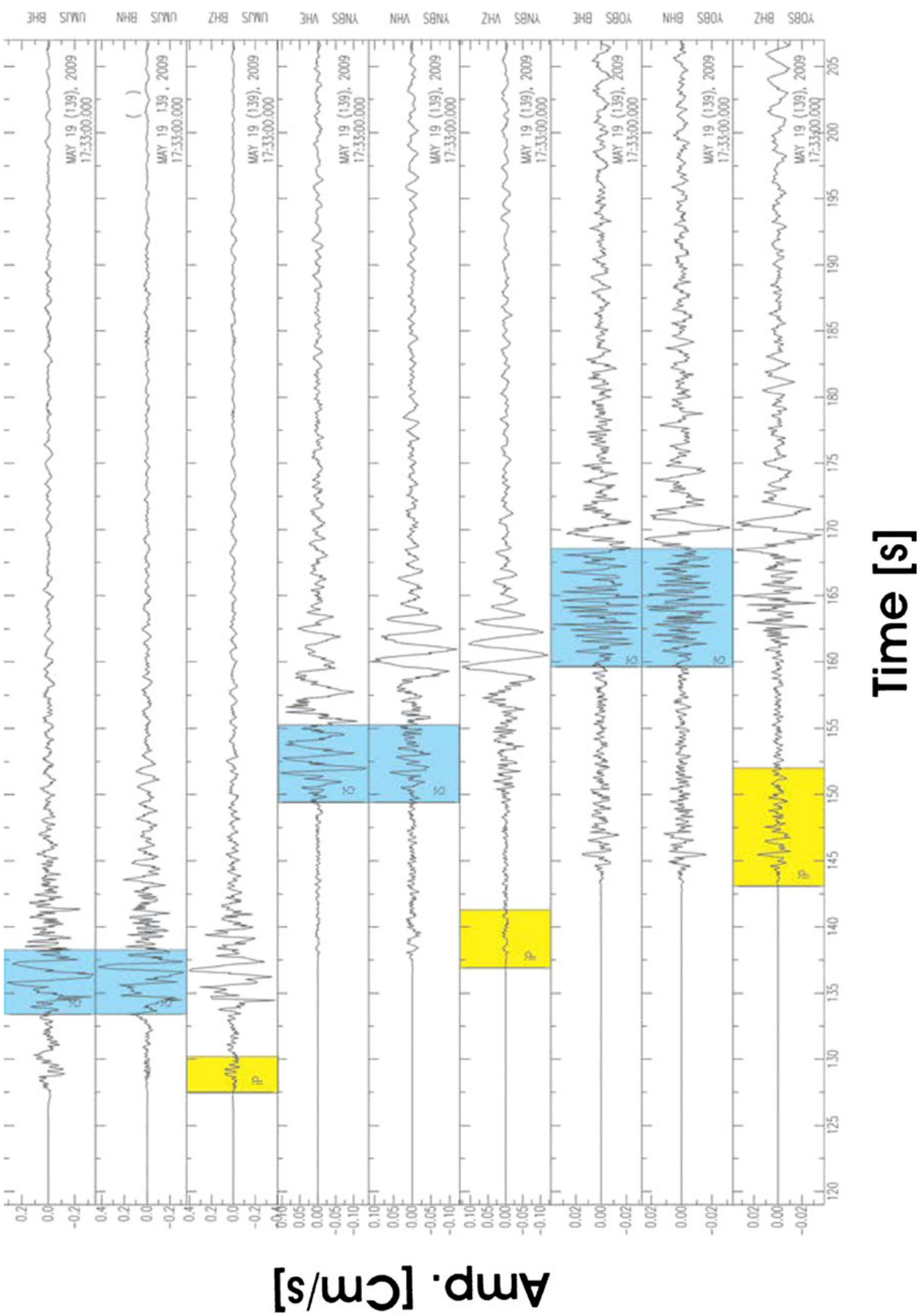

Fig. 5 Three component seismograms for the mainshock occurred on 19 May 2009. The traces are aligned after 1 s from the origin time of the event. Station codes and components are shown at the *right end* of each trace. Shadow windows refer to P wave (*yellow*) and S wave windows (*light blue*) used in spectral parameter estimations

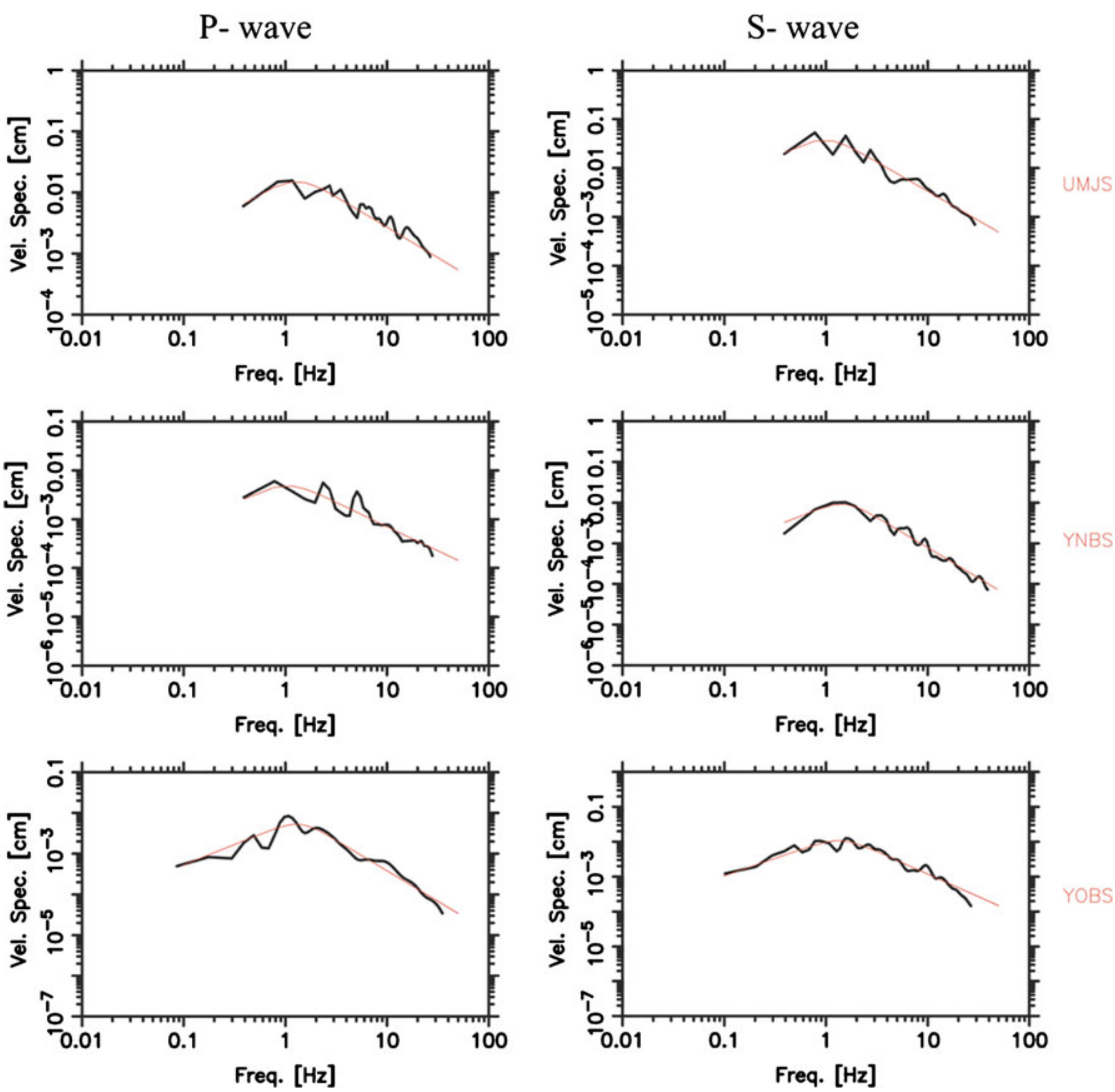

Fig. 6 The velocity spectra (*black solid line*) and the synthetic spectra (*red solid line*) for P and S waves of the mainshock recorded by three permanent seismic stations, UMJS, YNBS and YOBS, operated by SGS

introducing into the relationships given by Brune (1970) and Hanks and Wyss (1972):

$$M_0 = 4\pi\rho\upsilon^3 R \frac{\Omega_0}{FR_{\theta,\varphi}} \tag{9}$$

$$r = \frac{2.34\upsilon}{2\pi f_0} \tag{10}$$

$$\Delta\sigma = \frac{7M_0}{16r^3} \tag{11}$$

Table 2 Averaged source parameters of the study events with their correspondent error factors

ID	M_0 [Nm]	E_{Mo}	r [m]	E_r	$\Delta\sigma$	$E_{\Delta\sigma}$	M_w	E_{Mw}
1	2.34E+14	1.98	369	1.29	21.63	2.15	3.5	1.05
2	7.80E+14	2.51	580	1.60	19.00	1.97	3.8	1.07
3	2.83E+16	1.42	1,498	1.54	32.00	1.70	4.8	1.06
4	1.78E+15	2.75	928	1.40	08.72	1.46	4.0	1.07

where ρ is the density of the medium (2.75 g/cm^3), υ is the wave velocity, d is the hypocentral distance, F is the free surface corrections (1 and 2 for P and S waves, respectively, García et al. 1996) and $R_{\theta,\phi}$ is the radiation pattern coefficient.

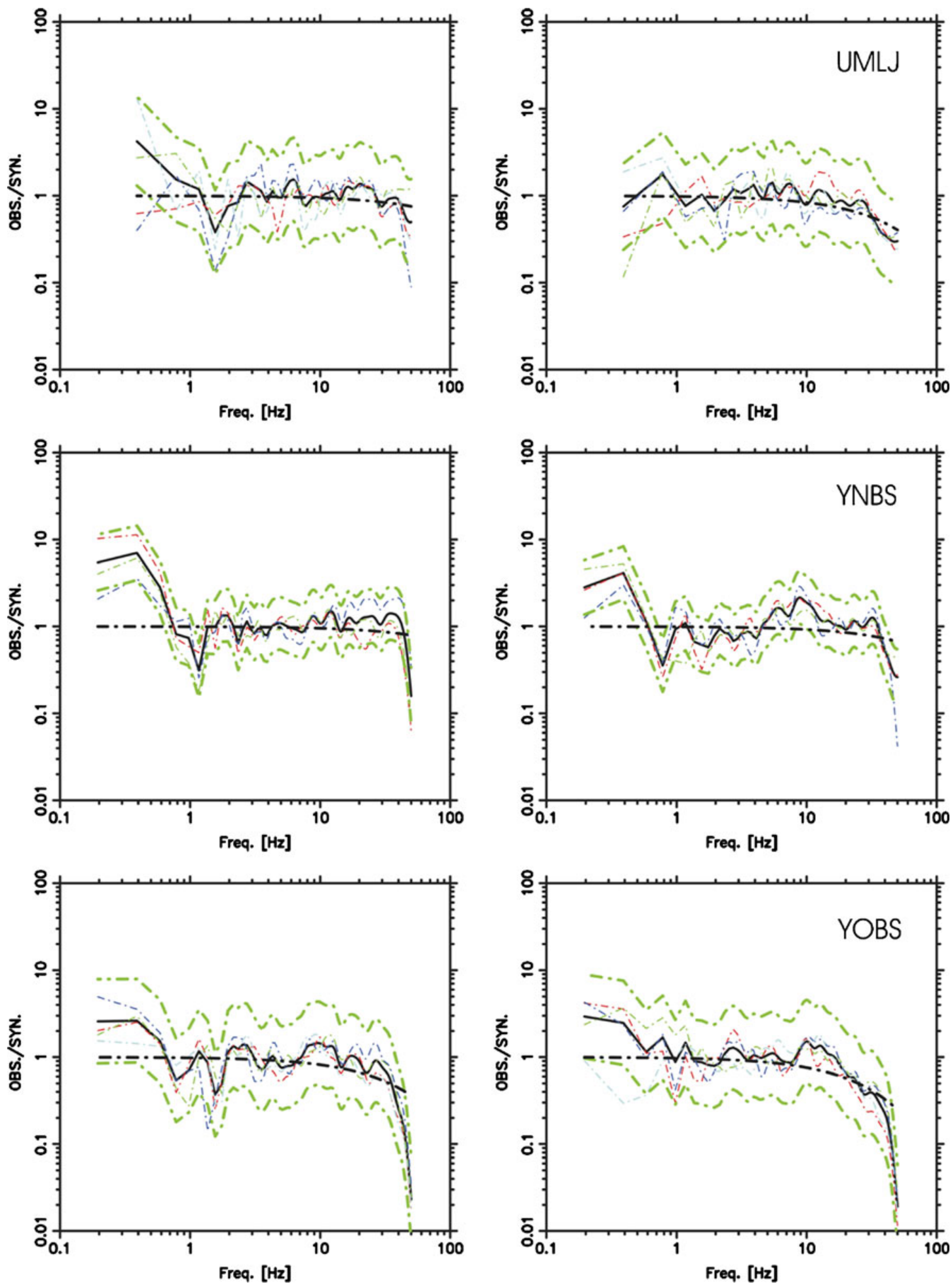

Fig. 7 Ratio between observed and synthetic spectra (*light blue*, *red*, *blue* and *green dotted lines*). Average ratio between observed and computed spectra displays by *black solid line*. *Black dashed line* shows attenuation curve assuming a frequency-independent Q. *Green dashed lines* represent ±1.0σ standard error interval

The velocity model derived by Rodgers et al. (1999) was used for seismic velocities (P and S waves) and the correspondent density. The root mean square averages of 0.52 and 0.63 were used for the P and S waves, respectively (Aki and Richards 1980). The average values for seismic moment, source radius and stress drop were computed (Table 2) at different stations following Archuleta et al. (1982):

$$\overline{x} = \text{antilog}\left(\frac{1}{N}\sum_{i=1}^{N}\log x_i\right) \tag{12}$$

where N is the number of stations used because the errors associated with Ω_0 and r are log-normally distributed. The standard deviation of the logarithm, $\mathrm{SD}(\log(\overline{x}))$, was estimated by calculating the variance of the individual logarithms about the mean logarithm:

$$\mathrm{SD}\left(\log\overline{x}\right) = \left(\frac{1}{N-1}\sum_{i=1}^{N}\sqrt{\left(\log x_i - \log\overline{x}\right)^2}\right) \tag{13}$$

and multiplicative error factors, E_x, were calculated as:

$$E_x = \text{antilog}(\mathrm{SD}(\log(x))) \tag{14}$$

On the other hand, the averaged attenuation effect in Eq. (2) would be calibrated as a function of anelastic attenuation $\exp(-\pi ft/Q)$ along the source–station path. By taking the ratio between observed and synthetic spectra, we can derive attenuation curves for P and S waves as shown in Fig. 7. The results obtained from the spectral ratio, as listed in Table 3, exhibited quality factors of P and S waves along the available source–station paths in the present study as shown in Fig. 8.

Note that the attenuation of seismic waves corresponding to the site effect, which is commonly included in Eq. (2) by multiplying the right hand side by $e^{-\pi kf}$ (e.g. Singh et al. 1982; Anderson and Hough 1984), is ignored in this study. However, when enough waveform data of good signal-to-noise ratio become available, the averaged site effect can be extracted from the residual remains from the deconvolution of the source and the observed amplitude spectra.

Discussions and conclusions

We estimated the source radius, seismic moment and stress drop of the four larger events of the Al-Ays 2009 earthquake swarm using spectral amplitudes. The data used were separately analysed for two successive time windows containing P and S waves.

Table 3 Quality factors of P and S waves along the available source–station paths

Station	Q_α	Q_β
UMJS	2,800	1,410
YNBS	2,060	2,590
YOBS	6,790	6,530

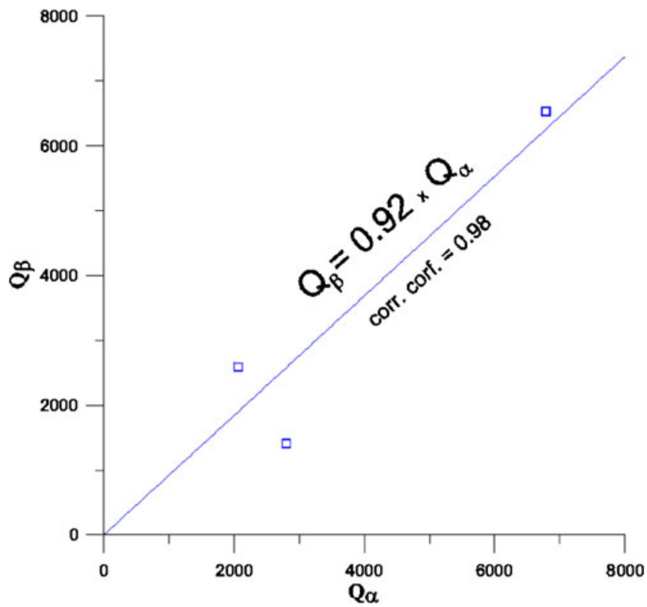

Fig. 8 The relation between the quality factors of P and S waves along the available source-station paths

The spectral parameters were obtained by fitting P wave and S wave spectrum with the theoretical model for velocity spectra as expressed by Eq. (3) and then they used to calculate the source parameters. Calculations were made using P and S wave data combined. For each event, the average values for the calculated source parameters are listed in Table 2. The calculated seismic moments ranged from 2.34E+14 to 2.83E+16 Nm and the corresponding moment magnitudes are 3.5 to 4.8; the fault radii were between 0.37 and 1.50 km and the stress drops spanned from 8.7 to 32.0 b. The mainshock moment magnitude obtained from the present study consistent with that determined by Craig et al. (2011) while it is different from the magnitude determined by the Harvard and SGS. The discrepancy may be due to uncertainties in the preliminarily estimation of magnitudes.

The present results exhibited that stress drops increase with the seismic moment and fault radius as already observed for tectonic earthquakes. The stress drops for the respective events are smaller than the usual values of type III intraplate earthquakes (mid-plate) but similar to type II intraplate earthquakes related to plate boundary (Schloz 1990). The low stress drops and large fault lengths may be due to the coupling of tectonic movements along the Red Sea rifting and upwelling fluids beneath the Arabian Shield which control a reactivation process of preexisting zones of weakness within the epicentral area.

It is worth stressing that the previous studies of Al-Damegh et al. (2004), Sandvol et al. (2007) and Pasyanos et al. (2009)

concluded that the Arabian Shield is characterised by a low attenuation effect on the propagation of the seismic waves. Although the observed spectral shapes are not essentially affected by low anelastic attenuation in the shield, they are in contrast with Brune's (1970) source model. The results showed that the spectral slopes, beyond the corner frequency, displayed $\omega^{-2.4}$, $\omega^{-2.5}$ and $\omega^{-2.6}$ (with an average of $\omega^{-2.5}$) along the source-to-station paths for the UMJS, YNBS and YOBS stations, respectively. It is worth stressing that high-frequency spectral slopes are not caused by local site effects and do not depend on the focal depth. So, we conclude that the obtained fall-off slopes may be attributed to the source effect (Brune et al. 1986; Iio 1986; Patanè et al. 1994). More detailed investigations on large data sets are required to distinguish the behaviour of high-frequency spectral slopes beyond the corner frequency.

The focal mechanisms of Al-Ays, Badr and Tabuk earthquakes (Fig. 3) exhibited pure normal mechanisms with two nodal planes trending NW-SE of NE-SW extensional stress field developed through the Arabian Shield as a consequence of the prevailing NW-SE extensional stress regime resulting from rifting process in the Red Sea. The dyke intrusion model of Al-Ays earthquake sequence, as proposed by Mukhopadhyay et al. (2012), inferred a seismic volume trending NW-SE bounded on both sides by two NW-SE trending fault systems dipping opposite to each other to form a nascent rift. Based on the geological investigations, Roobol (2007) suggested that Red Sea passive margin is undergoing extension of normal faults dipping towards and away from the Red Sea rift that might cause thinning of the Arabian Shield. As a matter of fact, the epicentral area is located approximately 60 km east of the passive Red Sea margin and might be controlled by the rifting process in the Red Sea. From the aforementioned tectonic scenarios, the source parameters obtained from the present study reveal that the type II intraplate earthquakes probably represent seismic source zones occurring nearby Al-Ays dislocation zone. However, at this stage, the inadequate waveform data cannot support to generalise the results for the entire region. This finding can be representative for the entire region of the Arabian Shield once large waveform data sets are available from different earthquake source zones.

Estimates, of the frequency-independent attenuation factor (Q) along source-to-station paths, exhibit low attenuation with a constant Q value of 3,833 and 3,530 for P and S waves, respectively. This finding constrained with those previously estimated for Lg, Pn and Sn seismic waves, reflecting low attenuation characteristics in the propagation of the seismic waves along the source-to-station path in the Arabian Shield (Al-Damegh et al. 2004; Sandvol et al. 2007). In addition, the obtained results are in consistence with the attenuation tomography beneath the Arabian Shield as determined by Pasyanos et al. (2009). These values are more typical of the continental shield areas (Rhea 1984; Atkinson and Mereu 1992; Boatwright 1994).

The results of attenuation characteristics of P and S waves are in consistence with the geological conditions of the Arabian Shield where Precambrian metamorphic basement is exposed. The volcanic rocks are part of a discontinuous belt of lava fields (Harrat) distributed along the Arabian Shield from the Gulf of Aden to beyond the Sinai Peninsula (Coleman et al. 1983; Coleman 1984; Coleman and McGuire 1988). As a consequence of tectonic process in the region, thinned continental crust extends offshore into the Red Sea from the Arabian Peninsula. From geological and geophysical studies summarised by Bohannon (1986) and Coleman and McGuire (1988), refraction data indicate that the continental crust beneath the western part of the Arabian Shield is about 40 km thick. It consists of a 20-km-thick upper layer having an average velocity of 6.3 km/s, a middle layer of 10 km thick which has an average velocity of 6.7 km/s and a lower layer in which the velocity increases from 6.8 to 7.3 to 7.8 km/s (Mooney et al. 1985; Gettings et al. 1986). The crust thins abruptly from about 40 km beneath the western margin of Precambrian outcrops of the Arabian Shield to about 18 km beneath the coastal plain in a horizontal distance of about 25 km. The thinning goes up to 8 km at a distance of 50 km offshore in the Red Sea (Plafker et al. 1987). From the aforementioned geological conditions, the occurrence of high-stress-release earthquakes within the continental Arabian Shield, where seismic attenuation is low, makes the intraplate earthquake potentially more damaging than its plate boundaries.

The obtained ratio of $Q_\beta/Q_\alpha \approx 0.9$ is slightly less than unity and reflects a slight departure from prefect elasticity because of the decreased rigidity along three source-to-station paths. The slight deviation of low Q_β/Q_α values might be in consistence with the upcoming rays intersecting the heterogeneous thermal anomalies that exist in the upper mantle which is suggested by many authors to be associated with the Cenozoic uplift of volcanic centres in the Arabian Shield. The presence of thermal anomalies may cause low attenuation for P waves than that for S waves in the Arabian Shield suggesting a dominant intrinsic attenuation mechanism in the lower crust of the Arabian Shield.

More studies are essential to investigate in detail the attenuation property of seismic waves in the upper crust of the swarm region. The structural weakening of the swarm region would be reflected on absorption attenuation due to injections of water and scattering attenuation due to cracks of various lengths in the region. These will emphasise our understanding on the attenuation mechanism of seismic waves in Al-Ays dislocation zone.

Acknowledgments The authors would like to thank Saudi Geological Survey for providing us with the available digital recordings used in the present study. Generic mapping tools by (Wessel and Smith 1991) are used to plot some of the figures in this manuscript. This project was supported by King Saud University, Deanship of Scientific Research, College of Science Research Centre. Two anonymous referees critically read the manuscript and provided us with helpful comments, which improved the manuscript

References

Adams RD, Barazangi M (1984) Seismotectonics and seismology in the Arab region: a brief summary and future plans. Bull Seismol Soc Am 74:1011–1030

Aki K, Richards G (1980) Quantitative seismology. W. H. Freeman, New York

Al-Amri A, Rodgers A, Al-Khalifah T (2008) Improving the level of seismic hazard parameter in Saudi Arabia using earthquake location. Arab J Geosci 1:1–15

Al-Damegh K, Sandvol E, Al-Lazki A, Barazangi M (2004) Regional seismic wave propagation (Lg and Sn) and Pn attenuation in the Arabian Plate and surrounding regions. GJI 157:775–795

Al-Damegh K, Sandvol E, Barazangi M (2005) Crustal structure of the Arabian plate: new constraints from the analysis of teleseismic receiver functions. Earth Planet Sci Lett 231:177–196

Al-Damegh K, Abou Elenean K, Hussein H, Rodgers A (2009) Earthquake sequence, Eastern Red Sea margin, Kingdom of Saudi Arabia. J Seismol. doi:10.1007/s10950-008-9148-5

Al-Damegh K, Hussein H, Al-Arifi N, Moustafa S, Moustafa M (2010) Focal mechanism of Badr earthquake, Saudi Arabia of August 27, 2009. Arab J Geosci. doi:10.1007/s12517-010-0200-8

Ambraseys NN, Melville CP, Adams RD (1994) The seismicity of Egypt, Arabia and Red Sea. Cambridge University Press, Cambridge

Anderson JG, Hough SE (1984) A model for the shape of the Fourier amplitude spectrum of acceleration at high frequencies. Bull Seismol Soc Am 74:1969–1993

Archuleta RJ, Cranswick EC, Mueller C, Spudich P (1982) Source parameters of the 1980 Mammoth Lakes, California, earthquake sequence. J Geophys Res 87:4595–4607

Atkinson GM, Mereu RF (1992) The shape of ground motion attenuation curves in Southeastern Canada. Bull Seismol Soc Am 82(5):2014–2031

Baer G, Hamiel Y (2010) Form and growth of an embryonic continental rift: InSAR observations and modelling of the 2009 western Arabia rifting episode. Geophys J Int 182:155–167

Benoti MH, Nyblade AA, Vandecar JC, Gurrola H (2003) Upper mantle P wave velocity structure and transition zone thickness beneath the Arabian Shield. Geophys Res Lett 30:1–4

Boatwright J (1978) Detailed analysis of two small New York State earthquake sequence. Bull Seismol Soc Am 68:1117–1131

Boatwright J (1994) Regional propagation characteristics and source parameters of earthquakes in northeastern North America. Bull Seismol Soc Am 84:1–15

Bohannon RG (1986) Tectonic configuration of the western Arabian continental margin, southern Red Sea. Tectonics 5:477–500

Bosworth W, Huchon P, McClay K (2005) The Red Sea and the Gulf of Aden Basins. J Afr Earth Sci 43: 334–378

Brune JN, Fletcher J, Vernon F, Haar L, Hanks T, Berger J (1986) Low stress-drop earthquakes in the light of new data from the Anza, California telemetered digital array. Am Geophys Monogr 37:237–245

Brown GF (1972) Tectonic map of the Arabian Peninsula, 1:4,000,000. Kingdom of Saudi Arabia, Ministry of Petroleum and Mineral Resources

Brune JN (1970) Tectonic stress and spectra of seismic shear waves from earthquakes. J Geophys Res 75:4997–5009

Camp VE, Roobol MJ (1992) Upwelling asthenosphere beneath western Arabia and its regional implications. J Geophys Res 97:15255–15271

Camp VE, Roobol MJ, Hooper PR (1991) The Arabian continental alkali basalt province: Part II, evolution of Harrats Khaybar, Ithnayn, and Kura, Kingdom of Saudi Arabia. Bull Geol Soc Am 103:363–391

Chang S-J, Van der Lee S (2011) Mantle plumes and associated flow beneath Arabia and East Africa. Earth Planet Sci Lett 302:448–454

Coleman RG (1984) The Red Sea: a small ocean basin formed by continental extension and sea floor spreading. Proc. 27th Intl. Geol. Cong, Moscow. 23: 93–121

Coleman RG, McGuire AV (1988) Magma systems related to the Red Sea opening. Tectonophysics 150(1–2):77–100

Coleman RG, Gregory RT, Brown GF (1983) Cenozoic volcanic rocks of Saudi Arabia. Saudi Arabian Deputy Ministry for Mineral Resources Open File Report, U.S. Geol. Surv., Open-File Rept. 0F-3-93, 82 pp

Craig TJ, Jackson JA, Priestley K, Mc Kenzie D (2011) Earthquake distribution patterns in Africa: their relationship to variations in lithospheric and geological structure, and their rheological implications. Geophys J Int 185:403–434

Daradich A, Mitrovica JX, Pysklywec RN, Willett SD, Forte AM (2003) Mantle flow, dynamic topography, and rift-flank uplift of Arabia. Geology 31:901–904

Debayle E, Leveque JJ, Cara M (2001) Seismic evidence for a deeply rooted low-velocity anomaly in the upper mantle beneath the northeastern Afro/Arabian continent. Earth Planet Sci Lett 193:423–436

García JM, Vidal F, Romacho MD, Martín-Marfil JM, Posadas A, Luzón F (1996) Seismic source parameters for microearthquakes of the Granada basin (southern Spain). Tectonophysics 261:51–66

Gettings ME, Blank HR, Mooney JWD, Healy JH (1986) Crustal structure of southwestern Saudi Arabia. J Geophys Res 91:6491–6512

Gillard D, Rubin AM, Okubo P (1996) Highly concentrated seismicity caused by deformation of Kilauea's deep magma system. Nature 384:343–346

Got J-L, Frechet J, Klein FW (1994) Deep fault plane geometry inferred from multiplet relative relocation beneath the south flank of Kilauea. J Geophys Res 99:375–386

Hanks T, Wyss M (1972) The use of body-wave spectra in the determination of seismic-source parameters. Bull Seismol Soc Am 62:561–589

Iio Y (1986) Scaling relation between earthquake size and duration of faulting for shallow earthquakes in seismic moment between 10^{10} and 10^{25} dyne cm. J Phys Earth 34:127–169

Imanishi K, Ellsworth W, Prejean S (2004) Earthquake source parameters determined by the SAFOD Pilot Hole seismic array. Geophysical Research Letters 31(12): doi:10.1029/2004GL019420

Julia J, Ammon C, Herrmann R (2003) Lithosphere structure of the Arabian Shield from the joint inversion of receiver functions and surface-wave group velocities. Tectonophysics 371:1–21

Konno K, Ohmachi T (1998) Ground-motion characteristics estimated from spectral ratio between horizontal and vertical components of microtremor. Bull Seismol Soc Am 88:228–241

Mooney WD, Gettings ME, Blank HR, Healy JH (1985) Saudi Arabian seismic deep refraction profiles: a travel time interpretation of deep crustal structure. Tectonophysics 111:173–246

Moufti MRH, Hashad MH (2005) Volcanic hazards assessment of Saudi Arabian Harrats: geochemical and isotopic studies of selected areas of active Makkah-Madinah-Nafud (MMN) volcanic rocks. Final Project Report (LGP-5-27). King

Abdlaziz City for Science and Technology, Riyadh, Saudi Arabia
Mukhopadhyay B, Mogren S, Mukhopadhyay M, Dasgupta S (2012) Incipient status of dyke intrusion in top crust—evidences from the Al-Ays 2009 earthquake swarm, Harrat Lunayyir, SW Saudi Arabia. Geomatics, Natural Hazards and Risk 1–19
Nyblade A, Park Y, Rodgers A, Al-Amri A (2006) Seismic structure of the Arabian Shield lithosphere and Red Sea margin, MARGINS Newsletter no. 17, p 13
Pallister JS, McCausland WA, Jónsson S, Lu Z, Zahran HM, El Hadidy S, Aburukbah A, Stewart ICF, Lundgren PR, White RA, Moufti MRH (2010) Broad accommodation of rift-related extension recorded by dyke intrusion in Saudi Arabia. Nat Geosci 3: doi:10.1038/NGEO966
Park Y, Nyblade AA, Rodgers AJ, Al-Amri AM (2007) Upper mantle structure beneath the Arabian Peninsula and northern Red Sea from teleseismic body wave tomography: implications for the origin of Cenozoic uplift and volcanism in the Arabian Shield. Geochem, Geophys, Geosyst 8(6): doi:10.1029/2006GC001566
Park Y, Nyblade AA, Rodgers AJ, Al-Amri AM (2008). S wave velocity structure of the Arabian Shield upper mantle from Rayleigh wave tomography. Geochem, Geophys, Geosyst 9: doi:10.1029/2007GC001895
Pasyanos ME, Walter WR, Matzel EM (2009) A simultaneous multiphase approach to determine P-wave and S-wave attenuation of the crust and upper mantle. Bull Seismol Soc Am 99(6):3314–3325
Patanè D, Privitera E, Ferrucci F, Gresta S (1994) Seismic activity leading to the 1991–1993 eruption of Mt. Etna and its tectonic implications. Acta Vulcanol 4:47–55
Plafker G, Agar R, Asker AH, Hanif M (1987) Surface effects and tectonic setting of the 13 December 1982 North Yemen earthquake. Bull Seismol Soc Am 77:2018–2037
Poirier JP, Taher M (1980) Historical seismicity in the near and middle east, North Africa, and Spain from Arabic documents (VIIth-XVIIIth century). Bull Seismol Soc Am 70:2185–2201
Rhea S (1984) Q determined from local earthquakes in the South Carolina Coastal Plain. Bull Seismol Soc Am 74:2257–2268
Rodgers A, Walter W, Mellors R, Al-Amri A, Zhang Y (1999) Lithospheric structure of the Arabian Shield and Platform from complete regional waveform modelling and surface wave group velocities. Geophys J Int 138:871–878
Roobol J (2007) Cenozoic faults in Western Saudi Arabia. In: 7th meeting of the Saudi society for geosciences, King Saud University, Riyadh, Saudi Arabia
Rubin AM, Gillard D, Got JL (1998) A reinterpretation of seismicity associated with the January 1983 dike intrusion at Kilauea Volcano, Hawaii. J Geophys Res 103:10003–10015
Rubin AM, Gillard D, Got JL (1999) Streaks of microearthquakes along creeping faults. Nature 400:635–641
Sandvol EA, Xueyang B, Zor E, Xie J, Mitchell BJ, Schaff DP (2007) Lg and Pg attenuation in the Middle East. 29th Monitoring Research Review: ground-based nuclear explosion monitoring. Technologies 266–273
Schloz CH (1990) The mechanics of earthquake faulting, Cambridge University Press, Cambridge, pp. 326–329
Singh SK, Apsel R, Fried J, Brune JN (1982) Spectral attenuation of SH waves along the Imperial fault. Bull Seismol Soc Am 72:2003–2016
Snoke JA (1987) Stable determination of (Brune) stress drops. Bull Seismol Soc Am 77(2):530–538
Stern RJ, Johnson P (2010) Continental lithosphere of the Arabian Plate: a geologic, petrologic, and geophysical synthesis. Earth Sci Rev 101:29–67
Vidale JE, Shearer PM (2006) A survey of 71 earthquake bursts across southern California: exploring the role of pore fluid pressure fluctuations and aseismic slip as drivers. JGR 111, B05312. doi:10.1029/2005JB004034
Waldhauser F, Ellsworth WL, Cole A (1999) Slip-parallel seismic lineations on the Northern Hayward fault, California. Geophys Res Lett 26:3525–3528
Wessel P, Smith W (1991) Free software helps maps and display data. EOS Trans Am Geophys Union 72:441